CHEMISTRY OF MATERIALS

ARTICLE

pubs.acs.org/cm

Deactivation and Regeneration of Oxygen Reduction Reactivity on Double Perovskite $Ba_2Bi_{0.1}Sc_{0.2}Co_{1.7}O_{6-x}$ Cathode for Intermediate-Temperature Solid Oxide Fuel Cells

Wei Zhou,[†] Jaka Sunarso,[‡] Julius Motuzas,[§] Fengli Liang,[†] Zhigang Chen,[∥] Lei Ge,[†] Shaomin Liu,[⊥] Anne Julbe,[§] and Zhonghua Zhu*[,†]

[†]School of Chemical Engineering and [∥]School of Materials Engineering and Centre for Microscopy and Microanalysis, University of Queensland, Brisbane, Queensland 4072, Australia

[‡]Australian Research Council (ARC) Centre of Excellence for Electromaterials Science, Institute for Technology Research and Innovation, Deakin University, Burwood, Victoria 3125, Australia

[§]Institut Europeen des Membranes, Universite Montpellier 2 (CC 47), Place Eugene Bataillon 34095, Montpellier Cedex 5, France

[⊥]Department of Chemical Engineering, Curtin University of Technology, Perth, Western Australia 6845, Australia

Supporting Information

ABSTRACT: in situ high-temperature X-ray diffraction and thermal gravimetric−differential thermal analysis on room-temperature powder, as well as X-ray diffraction, Raman spectroscopy, and transmission electron microscopy on quenched powder, were applied to study crystal structure and phase transformations in $Ba_2Bi_{0.1}Sc_{0.2}Co_{1.7}O_{6-x}$ (BBSC). Heating BBSC in air to over 800 °C produces a pure cubic phase with space group $Fm\bar{3}m$ (no. 225), and cooling down below 800 °C leads to a mixture of three noncubic phases including an unknown phase between 200 and 650 °C, a 2H hexagonal $BaCoO_3$ with space group $P63/mmc$ (no. 194) between 600 and 800 °C, and an intermediate phase at 800 °C. These three phases exist concurrently with the major cubic phase. The weight gain and loss between 300 and 900 °C suggest the occurrence of cobalt reduction, oxidation, and disproportion reactions with dominant reduction reaction at above 600 °C. The thermal expansion of BBSC was also examined by dilatometry. BBSC has a highly temperature-dependent thermal expansion coefficient which relates well with its structure evolution. Furthermore, the oxygen reduction reaction (ORR) of BBSC was probed by symmetrical cell and three-electrode configurations. The presence of hexagonal phase at 700 °C rarely affects the ORR performance of BBSC as evidenced by a slight increase of its area-specific resistance (ASR) value following 48 h of testing in this three-electrode configuration. This observation is in contrast to the commonly held point of view that noncubic phase deteriorates performance of perovskite compounds (especially in oxygen transport applications). Moreover, cathodic polarization treatment, for example, current discharge from BBSC (tested in three-electrode configuration), can be utilized to recover the original ORR performance. The cubic structure seems to be retained on the cathodic polarization—the normal cathode operating mode in fuel cells. Stable 72-h performance of BBSC in cathodic polarization mode further confirms that despite the presence of phase impurities, BBSC still demonstrates good performance between 500 and 700 °C, the desired intermediate operating temperature in solid oxide fuel cells.

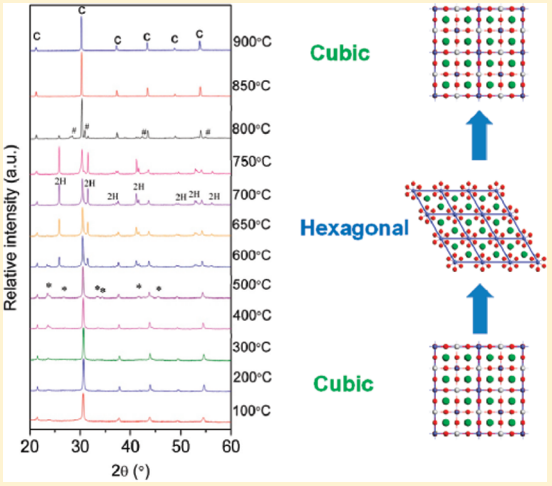

KEYWORDS: solid oxide fuel cells, perovskite, phase transition, hexagonal structure, oxygen reduction reaction

INTRODUCTION

Mixed ionic and electronic conductors (MIECs) based on $BaCoO_{3-\delta}$ perovskites are receiving renewed interest as cathodes for intermediate-temperature solid oxide fuel cells (IT-SOFCs) and oxygen-permeable membranes.[1−10] Particularly, cubic-structured $Ba_{0.5}Sr_{0.5}Co_{0.8}Fe_{0.2}O_{3-\delta}$ (BSCF) perovskite occupies a prominent position in the family of $BaCoO_{3-\delta}$ perovskites due to the large amount of mobile oxygen defects contained in its highly symmetric perovskite lattice. In recognition of its attractive oxygen ionic transport performance and oxygen reduction reaction (ORR) activity, BSCF was developed as an oxygen separation membrane in 2000[1] and applied as cathode material for a solid oxide fuel cell operated at intermediate temperatures (500−700 °C) in 2004.[2]

Received: December 12, 2010
Revised: January 31, 2011
Published: February 28, 2011

dx.doi.org/10.1021/cm103534x | *Chem. Mater.* 2011, 23, 1618–1624

In addition to high oxygen permeability and electrolytic ORR activity, good phase stability during operation is also important to ensure the compliance of cathode material with its industrial application. In this respect, BSCF also demonstrates stable structure at temperature above 900 °C.[11,12] However, operating BSCF at temperatures below 900 °C promotes its cubic to hexagonal structure transition.[11] For example, the oxygen flux performance of BSCF was reported to decay from its initial value by 50% after 240 h of operation at 750 °C.[13] This performance deterioration is attributed to the growth of hexagonal phase, which exhibits low ionic and electronic conductivities.

BSCF structural instability at intermediate temperature is explained by Švarcová et al.[14] in terms of the oxidation of B-site cations (B is transition metal and corresponds to B in $ABO_{3-\delta}$) which leads to its reduced ionic radius and increased Goldschmidt tolerance factor. Further on, Arnold et al.[12] confirm, by electron energy loss spectroscopy, the change in the valence state of cobalt, which accounts for 80 mol % of B-site cation on BSCF above 500 °C.

Partial substitution of A-site cation (Ba) in $BaCoO_{3-\delta}$ by other cations with smaller ionic radius, such as La and Sr, reduces the ionic radius discrepancy between A-site and B-site cations so that a lower tolerance factor can be obtained and the cubic structure is stabilized.[14] Normally, a larger content of A-site dopants, for example, more La or Sr, provides greater cubic structure stability.[15] Similarly, partial substitution of the B-site cation (Co) in $BaCoO_{3-\delta}$ by other metal cations with larger ionic radius can be utilized. Extensive studies have been devoted to the first approach with less attention given to the second approach, though recently, several Ba fully occupying A-site perovskites were reported to show promising performance as oxygen transport membranes and SOFC cathodes.[16−19] Moreover, high Ba content has been associated with enhanced oxygen transport property due to the formation of large lattice spacing.[20] For these reasons, we have developed Ba fully occupying A-site double perovskite, $Ba_2Bi_{0.1}Sc_{0.2}Co_{1.7}O_{6-x}$ (BBSC).[21] The presence of 5 mol % Bi and 10 mol % Sc in B-site on BBSC resulted in cubic structure at room temperature. Nevertheless, while BBSC demonstrates promising electrocatalytic ORR activity between 500 and 700 °C, questions remain about its structure and phase stability during long-term operation. In this work, in situ evolution of the crystal structure of BBSC is probed under normal working conditions of SOFC cathode: in air between 50 and 900 °C. Thermal gravimetric−differential thermal analysis and Raman spectroscopic data are presented to complement X-ray diffraction (XRD) data. We also provide detailed study on the ORR performance of BBSC, particularly on its deactivation with increasing operation hours. In addition, the possibility to regenerate the original ORR performance by cathodic polarization is also demonstrated.

EXPERIMENTAL SECTION

Sample Preparation. BBSC powder was synthesized by a combined ethylenediaminetetraacetic acid (EDTA)−citrate complexing process. $Ba(NO_3)_2$ (99.99+%, Sigma−Aldrich), $Bi(NO_3)_3\cdot 5H_2O$ (99.99+%, Sigma−Aldrich), $Sc(NO_3)_3$ (99.9%, Metall Rare Earth Limited, China), and $Co(NO_3)_2\cdot 6H_2O$ (98.0+%, Sigma−Aldrich) were used as the raw materials for metal sources. Stoichiometric amounts of these metal nitrates were mixed in deionized water and heated at 80 °C. Dissolution of $Bi(NO_3)_3\cdot 5H_2O$ was performed by adding the required amount of HNO_3 (67%). EDTA (99.9%, Sigma−Aldrich) and anhydrous citric acid (99.5%, Fluka) were then added as the complexing agents. The molar ratio of total metal nitrates, EDTA, and citric acid in the solution was 1:1:2. To ensure complete complexation, solution pH was adjusted to 6 by adding NH_3 aqueous solution (28%), resulting in a violet transparent aqueous solution. After evaporation of water at 120 °C, a dark purple gel was recovered. The gel was pretreated in the furnace at 250 °C for 8 h in air to form a solid precursor. The solid precursor was then ground into powder and calcined in air at 1050 °C for 5 h. The calcined powder was ball-milled in a planetary mill (Pulverisette 5, Fritsch) at 800 rpm for 2 h before characterization and testing.

Characterization. Pananalytical X-Pert Pro X-ray apparatus with an in situ heating accessory (HT-XRD, HT1200) and Cu Kα radiation was utilized to determine the structural evolution of powders during a temperature cycle from 100 to 900 °C in air with a heating rate of 5 °C·min^{-1}. The sample was stabilized by leaving it for 10 min at target temperature before each analysis. Le Bail and Rietveld refinements on the XRD patterns were carried out using DIFFRAC^{plus} Topas 4.2 software.[22] During refinements, general parameters, such as the scale factor, background parameters, and the zero point of the counter were optimized. Profile shape calculations were carried out by use of the Thompson−Cox−Hastings function implemented in the program by varying the strain parameter. Thermal gravimetric (TG)−differential thermal analysis (DTA) curves in air were simultaneously obtained in a TGA−DSC apparatus 2960 SDT V3.0F. Analyses were carried out under air flow rate of 20 mL·min^{-1} between room temperature and 900 °C at ramping and cooling rate of 2 °C·min^{-1}. Raman spectra were recorded in the backscattering mode at room temperature on a Renishaw inVia micro-Raman system equipped with an optical microscope comprising a 50× objective lens. The radiation source was a He−Ne laser with beam of wavelength 780 nm operated at 1% power, which was focused on a spot of 5 μm in size at 1.0 mW. Before measurement, the micro-Raman system was calibrated with the 520 cm^{-1} peak of polycrystalline Si. Transmission electron microscopy (TEM) was conducted at 200 kV with a Philips Tecnai T30F field emission instrument equipped with a 2k charge-coupled device (CCD) camera. Energy dispersive X-ray spectroscopy (EDS) was carried out with a light-element detector via the ZAF technique. Thermal expansion data were collected with a dilatometer (Netsch DIL 402C/3/G) from room temperature to 900 °C on a 2 mm × 5 mm × 12 mm BSF bar (previously sintered at 1050 °C in air).

Electrochemical Tests. BBSC slurry for spray deposition was prepared by dispersing BBSC powder with a premixed solution of glycerol and isopropyl alcohol, followed by rapid mixing and milling in an agate mortar for 0.5 h. A symmetrical cell of electrode|$Sm_{0.2}Ce_{0.8}O_{1.9}$(SDC)|electrode configuration was fabricated by spraying BBSC slurry onto both surfaces of SDC disk in a symmetric configuration and calcining the sprayed cells in air at 950 °C for 2 h. A three-electrode setup was also fabricated to test the long-term stability and to perform the cathodic polarization on the BBSC cathode. BBSC slurry was painted on one side of SDC electrolyte disk to form an electrode area of 0.26 cm^2 as working electrode (WE). Silver paste was painted symmetrically on the opposite side of the SDC disk as a counterelectrode (CE). Silver paste was also painted in the circumferential surfaces of the disk as a reference electrode (RE). The gap between CE and RE is 3 times larger than the thickness of the electrolyte. The electrochemical impedance spectra (EIS) of the symmetric cell and three-electrode cell were obtained on an Autolab, PGSTAT30 electrochemical workstation. The frequency range was 0.1−100 kHz and the signal amplitude was 10 mV under open cell voltage conditions. The cathodic polarization was performed with a current of −1 A·cm^{-2}, where the negative value indicates current flow direction from WE to CE.

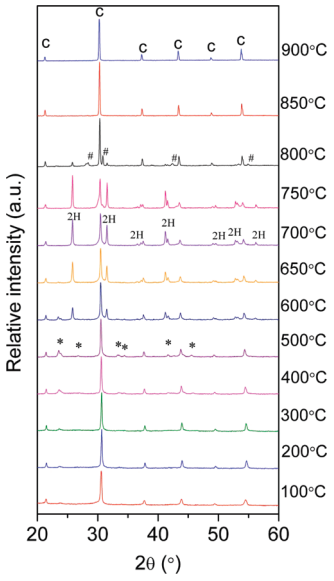

Figure 1. Thermal evolution of the XRD patterns collected in situ starting from BBSC cubic polymorph at 100 to 900 °C (C, cubic phase; *, unidentified phase; 2H, $BaCoO_3$; #, intermediate phases).

RESULTS AND DISCUSSION

The room-temperature structure of $Ba_2Bi_{0.1}Sc_{0.2}Co_{1.7}O_{6-x}$ (BBSC) is predominantly double cubic perovskite according to selected area electron diffraction patterns on TEM and Rietveld refinements on XRD results in our recent work.[21] The existence of Ba, Bi, Sc, and Co in nominal molar ratios (1:0.05:0.1:0.85) is confirmed by EDX spectra (Supporting Information, Figure S1). Similar molar ratios were also obtained on a BBSC sample previously at 900 °C, which indicates retaining of bismuth. Figure 1 shows the in situ XRD patterns of BBSC powders obtained upon heating up to 900 °C. At temperature above 800 °C, BBSC becomes a pure cubic phase. Below 800 °C, BBSC exists in a mixture, and the dominant phase has a cubic symmetry as denoted by the C symbols. An unknown phase denoted by asterisks starts to form at 200 °C, the amount of which increases with increasing temperature as indicated by increasing peak intensity until it reaches a maximum at 500 °C. This phase might belong to one of the $A(A'_yB_{1-2y})O_{3(1-y)}$ phases, whereby Co acts as both A′ and B cation while Ba acts as A cation as observed previously in Ba−Co−O perovskite systems.[23] Heating to above 500 °C leads to the reduction of its characteristic peak intensity until it completely disappears at 650 °C. Another phase then follows at 600 °C (denoted by 2H symbols), which can be indexed as $BaCoO_3$ according to ICDD−JCPDS card 70-0363.[24] Le Bail refinements were carried out on XRD patterns at 600−750 °C to confirm the existence of this phase (together with the main cubic phase C), which was identified as 2H hexagonal $BaCoO_3$ with the space group $P6_3/mmc$ (no. 194).[25] The refined lattice parameters are listed in Table 1, which also includes the obtained reliability factors of refinements. The refinements converge to reliability factors of $\chi^2 \leq 2.22$, $R_p \leq 3.06$, $R_{wp} \leq 4.33$, $R_{exp} = 1.95$, and $R_{Bragg} \leq 0.53$. Interestingly, increasing temperature from 600 to 750 °C causes symmetrical expansion of the cubic phase (increased *a*), while the hexagonal phase experiences height expansion (increased *c*) and hexagon surface shrinkage (decreased *a*) at the same time (Table 1).

The formation of hexagonal phase is also observed by high-resolution transmission electron micrograph (HR-TEM) of BBSC powder quenched at 700 °C (Figure 2). Quenching results in the presence of many streaks in the crystal lattices, which were not observed previously by HR-TEM on room-temperature BBSC powder.[21] These streaks were also observed on double perovskite $Ba_2Co_{1.5}Mo_{0.25}Nb_{0.25}O_{6-x}$ by Deng et al.,[17] which is attributed to the hexagonal $BaCoO_3$. To this end, the transition from cubic structure to its hexagonal polymorphs is likely to be facilitated via a shear of BaO_3 layers (according to Arnold et al.).[11] In the cubic symmetrical cell, BaO_3 layers are oriented perpendicularly to the [1 1 1] cubic zone axis to form cubic close packing and B cations occupy the octahedral holes with the octahedron, generating a three-dimensional corner-sharing array. Shearing of some BaO_3 layers here leads to the formation of hexagonal close packing and face-shared octahedral columns along [1 1 1] cubic orientation.

The ratio of 2H hexagonal to main cubic phase can be approximated by their relative peak intensity as displayed in Figure S2 (Supporting Information). The amount of 2H phase increases (at the expense of cubic phase) with increasing temperature from 600 to 750 °C. Notably, the intensity of 2H phase is reduced by heating up to 800 °C, accompanied by the occurrence of another intermediate phase denoted by 5H symbols. Most likely, the 2H phase transforms to cubic phase through this intermediate phase. This intermediate shows similar structure with 5−12H hexagonal $BaCoO_{3-\delta}$ ($2.43 < 3 - \delta < 2.74$).[26−28] The Co valence state in 5−12H hexagonal phase is lower than that in 2H phase, indicating that the hexagonal to cubic transition is attributed to the reduction of cobalt. In between 2H (*hhh*) and 3C (*ccc*) phases, polytypes that have different ratios of cubic to hexagonal stacking have been identified, namely, 9R (*chhchhchh*) 4H (*chch*), 6H (*cchcch*) and 12H (*ccchhh*) (where *c* and *h* denote cubic and hexagonal stacks, respectively). The hexagonal polytypes can be transformed to cubic gradually and vice versa, as noticed in the sequence case of 2H-9R-4H-6H-3C.[29] For example, the decomposition of cubic phase to 2H hexagonal phase in BSCF is facilitated by the formation of 6H hexagonal phase (reported by Arnold et al.).[11] Additionally, 5H (*ccchh*) hexagonal intermediate phase was also noted during decomposition of $BaIrO_3$ perovskite (reported by Cheng et al.).[30] At 850 °C, Figure 1 shows that the hexagonal phase completely transforms into cubic phase with $Fm\bar{3}m$ space group as verified by Rietveld refinement (using XRD patterns obtained at 850 and 900 °C), the fitting plots of which are provided as Figure 3. BBSC structure was modeled with Ba occupies 8c ($^1/_4$, $^1/_4$, $^1/_4$) positions, Co occupies 4a (0, 0, 0) and 4b ($^1/_2$, $^1/_2$, $^1/_2$) positions, Bi and Sc occupies 4b ($^1/_2$, $^1/_2$, $^1/_2$) positions, and O occupies 24e ($^1/_4$, 0, 0) positions (ICSD no. 189).[31] Table S1 (Supporting Information) lists the refined structure results and reliability factors. As expected, increasing cubic lattice size from 8.32 to 8.33 Å appears upon increasing temperature from 850 to 900 °C. Relatively low reliability factor values ($\chi^2 \leq 2.47$, $R_p \leq 4.38$, $R_{wp} \leq 5.98$, $R_{exp} \leq 2.42$, and $R_{Bragg} \leq 2.98$) indicate good fitting. The formation of cubic phase from hexagonal phase can be rationalized in terms of their distinct features. While BO_6 in cubic structure is corner-shared, BO_6 in hexagonal symmetry is face-shared. The distance between B-site cations in hexagonal structure is therefore shorter than in cubic structure. The reduction of Co cations increases its ionic radius, resulting in increased distance between B-site cations as well as destabilization of hexagonal structure.

Table 1. Two-Phase Le Bail Refinement Results for BBSC: Phases A and B[a]

	600 °C		650 °C		700 °C		750 °C	
	A	B	A	B	A	B	A	B
a (Å)	8.2697(0)	5.6700(7)	8.2794(5)	5.6695(6)	8.2875(8)	5.6658(2)	8.3163(5)	5.6632(4)
c (Å)		4.8184(0)		4.8266(8)		4.8315(5)		4.8375(6)
	600 °C		650 °C		700 °C		750 °C	
χ^2	2.10		1.95		1.98		2.22	
R_p (%)	2.94		2.78		2.80		3.06	
R_{wp} (%)	4.10		3.81		3.86		4.33	
R_{exp} (%)	1.95		1.95		1.95		1.95	
R_{Bragg} (%)	0.18		0.38		0.30		0.53	

[a] Phase A, cubic *Fm*-3*m* space group (no. 225); phase B, hexagonal *P*63/*mmc* space group (no. 194).

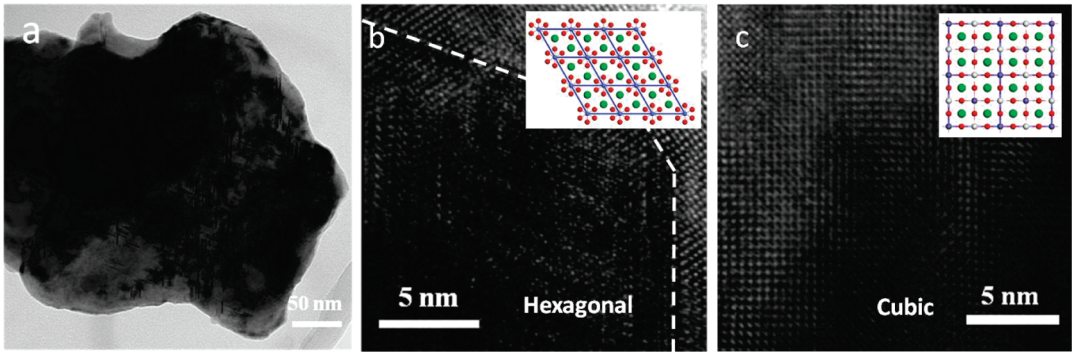

Figure 2. (a) Typical TEM image of BBSC quenched at 700 °C, and HRTEM of the quenched sample: (b) hexagonal phase and (c) cubic phase. Structural models are depicted in the insets.

The TG−DTA curves of BBSC powder are displayed in Figure 4. There is an abrupt weight loss (~6%) between room temperature and 240 °C, which is ascribed to the moisture removal and surface oxygen desorption followed by constant weight profile above 240 °C. The exothermic peak centered at 210 °C on the TGA curve is associated with the formation of unknown phase detected earlier by XRD (Figure 1). Subsequently, a gain of mass (~1%) (probably from oxygen sorption) is observed between 340 and 500 °C, indicating the increase in oxygen content and oxidation of cobalt. By further heating the powder to over 500 °C, continuous weight loss is noticed. In the temperature region where 2H hexagonal $BaCoO_3$ phase starts to form (around 600 °C), there is no clear correlating feature in the DTA curve. It is likely that this phase formation, accompanied by very small heat transfer, corresponds to a subtle order−disorder transformation.[32] Furthermore, the formation of 2H phase featured by high-valence cobalt cation (~4) (Figure 1) together with the weight loss occurrence between 600 and 750 °C, which involves cobalt reduction (Figure 4), implies the simultaneous existence of three reactions, oxidation, reduction, and disproportionation for Co cations, represented as eqs 1−3, respectively:

$$2Co_{Co}^{\times} + V_O^{\cdot\cdot} + \frac{1}{2}O_2 = 2Co_{Co}^{\cdot} + O_O^{\times} \quad (1)$$

$$2Co_{Co}^{\times} + O_O^{\times} = 2Co_{Co}^{\prime} + V_O^{\cdot\cdot} + \frac{1}{2}O_2 \quad (2)$$

$$2Co_{Co}^{\times} = Co_{Co}^{\cdot} + Co_{Co}^{\prime} \quad (3)$$

It can be reasoned that eq 2 is the dominant reaction between 600 and 750 °C as evidenced by the observed weight loss. The nonexistence of phase transition above 800 °C is consistent with the absence of endothermic/exothermic peaks on the DTA curve in the same temperature range.

The upward inflecting shape of the TGA curve around 500 °C indicates oxygen gain, which can be related to the formation of 2H phase. Nevertheless, this phase is not noticed in high-temperature XRD (Figure 1) until 600 °C. Relatively short dwelling time at each temperature during HT-XRD analysis (e.g., too short to reach equilibrium) as well as low sensitivity of XRD for phase detection at low concentrations has to be considered in order to retain high-temperature structure. Therefore, in this study, room-temperature BBSC powder was heated to 500 °C and kept at this temperature for 5 h before being quenched to room temperature and analyzed. Figure 5 depicts the XRD patterns of the quenched powder, which verify the existence of 2H phase as the third phase. Figure S3 (Supporting Information) compares the Raman spectra of the quenched and room-temperature BBSC powder. The characteristic peaks at Raman shift in excess of 200 cm^{-1} are associated with the rotational, bending, and stretching-like vibrations from CoO_6 octahedron.[33] Their appearance at 500 °C represents a structure with lower symmetry (relative to the room-temperature structure). In particular, the stretching mode peak at 690 cm^{-1} is related to the hexagonal phase, while peaks at 640 and 490 cm^{-1} are ascribed to the orthorhombic phase.[34]

The thermal expansion behavior of BBSC was measured in air. Figure 6 shows the thermal expansion curves as a function of

dx.doi.org/10.1021/cm103534x |*Chem. Mater.* 2011, 23, 1618–1624

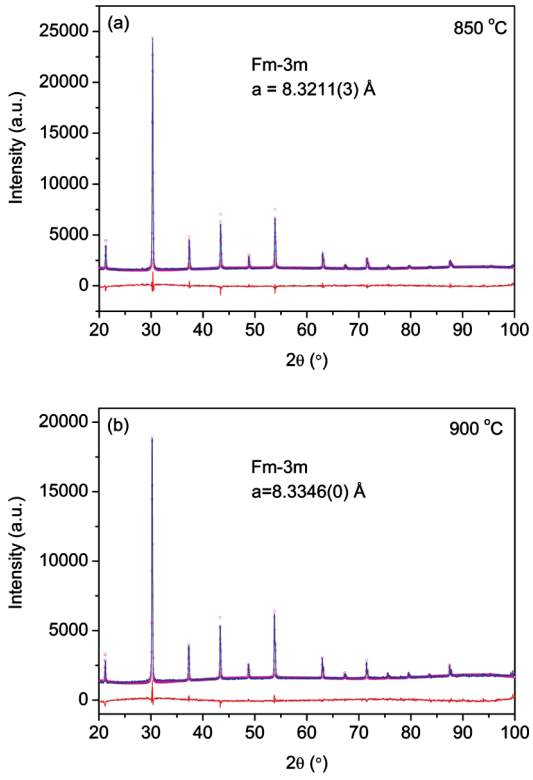

Figure 3. XRD patterns of BBSC annealed at (a) 850 °C and (b) 900 °C, fitted by use of the space group described in the text (the $Fm\bar{3}m$ space group). Observed (pink circles), calculated (blue solid line), and difference (red, bottom) profiles are shown.

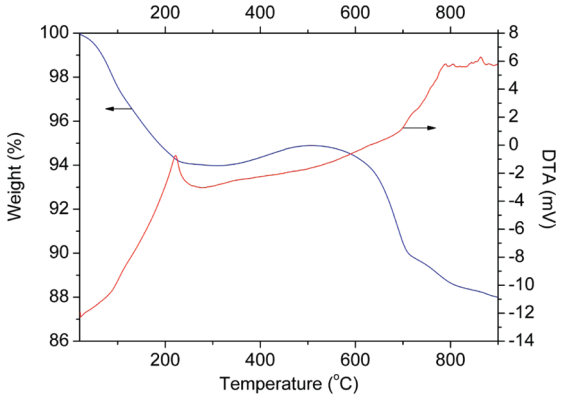

Figure 4. Thermal analysis curves recorded in air: TG (left axis) and DTA (right axis).

temperature from 25 to 900 °C. The thermal expansion coefficients (TECs) of BBSC are highly temperature-dependent, although relatively constant TECs values can be obtained in short temperature ranges listed in Table 2. They vary from a minimum value of $9.9 \times 10^{-6}\,K^{-1}$ to a maximum value of $26.9 \times 10^{-6}\,K^{-1}$. Consistent with the TG results between 340 and 450 °C (Figure 4), which show weight gain due to cobalt oxidation, the thermal expansion curve shows kinks at this temperature range corresponding to very low TEC values. This is attributed to lattice contraction since the Co ionic radius is reduced after oxidation. In parallel with 2H phase formation, the TECs increase gradually between 600 and 700 °C, implying

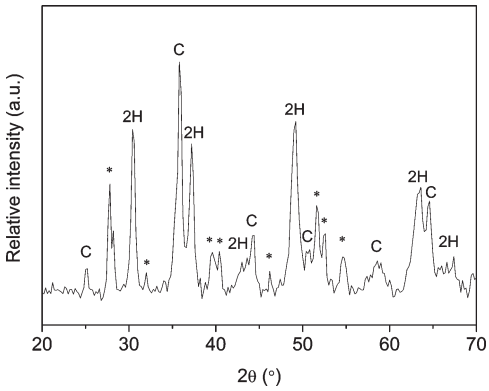

Figure 5. XRD pattern of BBSC quenched at 700 °C (C, cubic phase; *, unidentified phase; 2H, $BaCoO_3$).

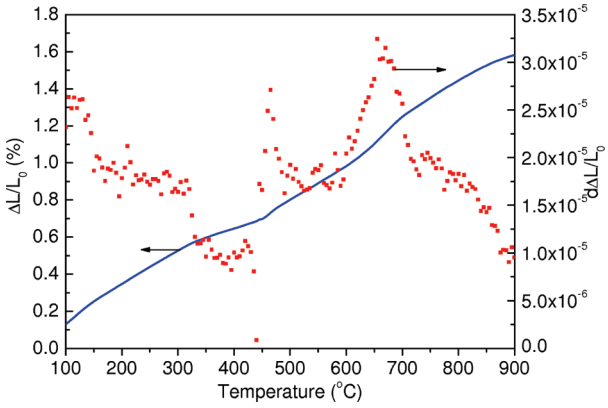

Figure 6. Thermal expansion behavior of BBSC.

Table 2. Thermal Expansion Coefficients of BBSC in Different Temperature Ranges

T (°C)	100−340	340−450	450−600	600−725	725−900
TEC ($\times 10^{-6}\,K^{-1}$)	18.9	9.9	18.6	26.9	16.4

cobalt reduction. Heating in excess of 700 °C leads to constantly decreasing TEC values.

Formation of hexagonal phase in perovskite compound is generally considered to deteriorate SOFC cathode performance at 500−700 °C since the phase transformation in $BaCoO_{3-\delta}$-based perovskites takes place below 800 °C.[11] Although the negative impact of hexagonal phase on the oxygen permeability has been reported frequently, its impact on the cathode performance has not been reported. Impedance spectroscopy measurements were performed on the symmetrical BBSC|SDC|BBSC cell between 450 and 850 °C with a heating and cooling rate of 5 °C·min^{-1}. Reaction between BBSC cathode and SDC electrolyte was probed by XRD on their powder mixtures fired between 900 and 1050 °C as depicted in Figure S4 (Supporting Information). Since relatively weaker phase reaction occurred for powder mixtures fired at 950 °C compared to those fired at 1000 °C, the former temperature is chosen as the firing temperature between BBSC and SDC. The temperature-dependent area-specific resistances (ASRs) (e.g., the difference between the low- and high-frequency intercepts of the real axis) are shown in Figure 7. Upon heating, the ASRs decrease linearly between 450 and 700 °C and more abruptly between 700 and 850 °C. Gradual

dx.doi.org/10.1021/cm103534x |*Chem. Mater.* 2011, 23, 1618–1624

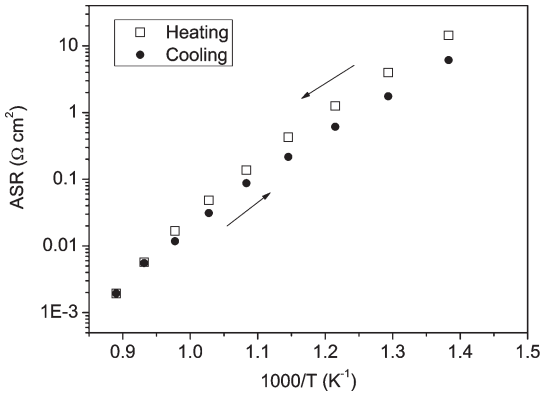

Figure 7. Temperature dependence of ASRs for BBSC cathode based on a symmetric cell.

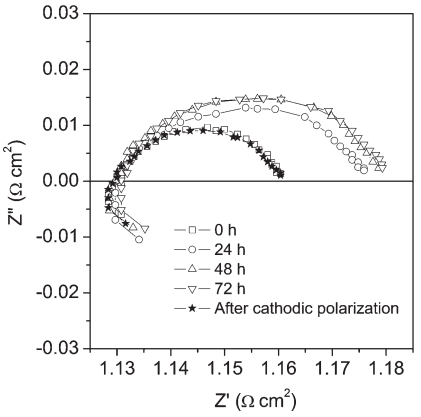

Figure 8. Impedance spectra of BBSC cathode based on a three-electrode cell obtained at different times at 700 °C, showing the instability and regeneration property of the material.

elimination of 2H phase starting from 750 °C might contribute to this substantial cathode performance improvement. On cooling down from 850 to 450 °C, lower ASRs (relative to the ASRs on heating) are obtained since BBSC retains its cubic structure as indicated by in situ XRD results taken upon cooling from 900 °C to room temperature (Figure S5, Supporting Information). Apparently, BBSC cubic phase is thermodynamically stable above 800 °C in air and can be maintained (most likely as a metastable phase) upon cooling to room temperature, provided that the cooling rate is fast enough to prevent its decomposition into hexagonal $BaCoO_3$. The difference in ASR magnitudes during heating and cooling confirms that hexagonal phase is detrimental to the ORR performance although such an effect is not pronounced. For example, at 700 and 750 °C, at which the hexagonal phase is dominant, the ASR gaps are only ~0.017 and ~0.005 $\Omega \cdot cm^2$, respectively.

Long-term performance of the BBSC cathode at 700 °C was also tested. Figure 8 displays the impedance spectra from a BBSC-based cell with three-electrode setup after 24, 48, and 72 h. The ASR increases by ~0.02 $\Omega \cdot cm^2$ after 48 h and stays constant afterward. Therefore, the presence of hexagonal $BaCoO_3$ phase rarely affects the cathode performance of perovskite compound, although the oxygen permeability was reported to decay by 50%.[13] The reason is due to the low electronic conductivity of hexagonal phase compared to the cubic phase. This is attributed to the difference in the mechanism of oxygen transport material,

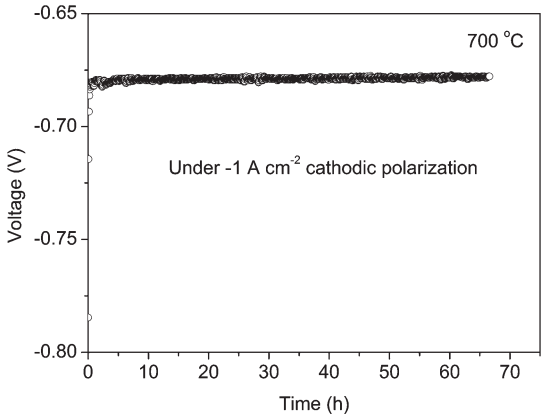

Figure 9. Voltage response (including ohmic resistance from electrolyte) of BBSC cathode under a constant current density of $-1\ A \cdot cm^{-2}$ at 700 °C.

which relies on mixed ionic−electronic conduction, whereas the cathode relies on the oxygen reduction reaction. In the former application, electron conduction in the material is crucial and limits the ionic transport rate. In the latter, however, the electrons are supplied from the external circuit.

The application of cathodic polarization for 0.5 h (e.g., introduction of $-1\ A \cdot cm^{-2}$ current from WE to CE) onto the BBSC cathode after heating at 700 °C for 72 h recovers the cathode performance to the original value (at 0 h) (Figure 8). It is highly probable that this polarization regenerates cubic structure from hexagonal phase formed upon staying at 700 °C for a long period. In some respect, cathodic polarization exhibits an effect similar to a reducing atmosphere by supplying electrons to the BBSC (which equals to discharging current from BBSC). The most prone element in BBSC upon reduction is the transition metal, cobalt. Cobalt reduction here provides a tendency toward cubic structure formation due to its larger ionic radius in reduced form. A similar finding, reduction−oxidation of Fe cations under anodic and cathodic polarization, was also reported by Nemudry et al.,[35] which promotes phase transition in $SrFeO_{2.5+x}$ perovskite. Co-cations in BBSC are likely to be electrochemically reduced (upon cathodic polarization) according to eq 4:

$$2Co_{Co}^{\times} + 2e^{-} = 2Co_{Co}^{'} + \frac{1}{2}O_2 \qquad (4)$$

In normal SOFC operating conditions, the current is discharged from the cathode, that is, cathodic polarized. Therefore, the formation of hexagonal phase is expected to be suppressed. To confirm this, voltage under cathodic polarization ($-1\ A \cdot cm^{-2}$) is monitored for 72 h (Figure 9). Very stable voltage response, without even slight increase over this time period, indicates that this is indeed the case.

CONCLUSIONS

HT-XRD study demonstrates that, upon heating up to 800 °C, BBSC consists of cubic phase, unknown phase, and several hexagonal phases. Increasing temperature in excess of 800 °C results in pure cubic structure. Upon cooling down from 900 to 100 °C, the cubic structure is retained, probably caused by the slow structural change kinetics. XRD and Raman spectroscopy on quenched BBSC powder indicate the existence of 2H hexagonal $BaCoO_3$ phase at temperature lower than 500 °C, which relates well with the weight gain observed in TGA in the

same temperature range. The highly temperature-dependent thermal expansion behavior of BBSC is also consistent with its phase evolution.

The impedance spectroscopy results of BBSC in symmetrical cell and three-electrode configurations at 700 °C show that the presence of hexagonal phase does not behave detrimentally toward the oxygen reduction reaction (ORR) performance. In addition, the application of cathodic polarization enables the regeneration of initial ORR performance and allows stable ORR performance over 72 h, most probably through cobalt reduction, which favors cubic structure formation and offsets the decomposition of cubic phase to hexagonal phase.

■ ASSOCIATED CONTENT

Supporting Information. Five figures and one table as described in the text. This material is available free of charge via the Internet at http://pubs.acs.org.

■ AUTHOR INFORMATION

Corresponding Author

*Tel +61 7 3365 3528; fax +61 7 3365 4199; e-mail z.zhu@uq.edu.au.

■ ACKNOWLEDGMENT

W.Z. appreciates the support of an Australian Research Council (ARC) Discovery Project (Grant DP1095089).

■ REFERENCES

(1) Shao, Z. P.; Yang, W. S.; Cong, Y.; Dong, H.; Tong, J. H.; Xiong, G. X. *J. Membr. Sci.* **2000**, *172*, 177.
(2) Shao, Z. P.; Haile, S. M. *Nature* **2004**, *431*, 170.
(3) Zhou, W.; Ran, R.; Shao, Z. P. *J. Power Sources* **2009**, *192*, 231.
(4) Harada, M.; Domen, K.; Hara, M.; Tatsumi, T. *Chem. Lett.* **2006**, *35*, 968.
(5) Li, Q. M.; Zhu, X. F.; He, Y. F.; Yang, W. S. *Catal. Today* **2010**, *149*, 185.
(6) Tong, J. H.; Yang, W. S.; Zhu, B. C.; Cai, R. *J. Membr. Sci.* **2002**, *203*, 175.
(7) Cheng, Y.; Zhao, H.; Teng, D.; Li, F.; Lu, X.; Ding, W. *J. Membr. Sci.* **2008**, *322*, 484.
(8) Burriel, M.; Casas-Cabanas, M.; Zapata, J.; Tan, H. Y.; Verbeeck, J.; Solís, C.; Roqueta, J.; Skinner, S. J.; Kilner, J. A.; Van Tendeloo, G.; Santiso, J. *Chem. Mater.* **2010**, *22*, 5512.
(9) Kim, J. H.; Cassidy, M.; Irvine, J. T. S.; Bae, J. *Chem. Mater.* **2010**, *22*, 883.
(10) Lin, Y.; Ran, R.; Chen, D. J.; Shao, Z. P. *J. Power Sources* **2010**, *195*, 4700.
(11) Arnold, M.; Gesing, T. M.; Martynczuk, J.; Feldhoff, A. *Chem. Mater.* **2008**, *20*, 5851.
(12) Arnold, M.; Xu, Q.; Tichelaar, F. D.; Feldhoff, A. *Chem. Mater.* **2009**, *21*, 635.
(13) Efimov, K.; Xu, Q.; Feldhoff, A. *Chem. Mater.* **2010**, *22*, 5866.
(14) Švarcová, S.; Wiik, K.; Tolchard, J.; Bouwmeester, H. J. M.; Grande, T. *Solid State Ionics* **2008**, *178*, 1787.
(15) Harvey, A. S.; Litterst, F. J.; Yang, Z.; Rupp, J. L. M.; Infortuna, A.; Gauckler, L. J. *Phys. Chem. Chem. Phys.* **2009**, *11*, 3090.
(16) Jiang, H. Q.; Wang, H. H.; Werth, S.; Schiestel, T.; Caro, J. *Angew. Chem., Int. Ed.* **2008**, *47*, 9341.
(17) Deng, Z. Q.; Smit, J. P.; Niu, H. J.; Evans, G.; Li, M. R.; Xu, Z. L.; Claridge, J. B.; Rosseinsky, M. J. *Chem. Mater.* **2009**, *21*, 5154.
(18) Zhu, C. J.; Liu, X. M.; Yi, C. H.; Pei, L.; Yan, D. T.; Niu, J. P.; Wang, D. J.; Su, W. H. *Electrochem. Commun.* **2009**, *11*, 958.
(19) Luo, H. X.; Tian, B. B.; Wei, Y. Y.; Wang, H. H.; Jiang, H. Q.; Caro, J. *AIChE J.* **2010**, *56*, 604.
(20) Shao, Z. P.; Xiong, G. X.; Cong, Y.; Yang, W. S. *J. Membr. Sci.* **2000**, *164*, 167.
(21) Zhou, W.; Sunarso, J.; Chen, Z. G.; Ge, L.; Motuzas, J.; Zou, J.; Wang, G. X.; Julbe, A.; Zhu, Z. H. *Energy Environ. Sci.* DOI: 10.1039/C0EE00451K.
(22) *DIFFRACplus TOPAS 4*; Bruker AXS GmbH, Karlsruhe, Germany, 2008.
(23) Darriet, J.; Elcoro, L.; El Abed, A.; Gaudin, E.; Perez-Mato, J. M. *Chem. Mater.* **2002**, *14*, 3349.
(24) ICDD PDF-2 Release 2008, Joint Committee on Powder Diffraction Standards (JCPDS)—International Centre for Diffraction Data (ICDD), Powder Diffraction File (PDF) database, Newtown Square, PA, 2008.
(25) Taguchi, H.; Takeda, Y.; Kanamaru, F.; Shimada, M.; Koizumi, M. *Acta Crystallogr.* **1977**, *B33*, 1299.
(26) Parras, M.; Varela, A.; Seehofer, H.; González-Calbet, J. M. *J. Solid State Chem.* **1995**, *120*, 327.
(27) Zanne, M.; Courtois, A.; Gleitzer, C. *Bull. Soc. Chim. Fr.* **1972**, 4470.
(28) Varela, A.; Parras, M.; Boulahya, K.; González-Calbet, J. M. *J. Solid State Chem.* **1997**, *128*, 130.
(29) Jin, C. Q.; Zhou, J. S.; Goodenough, J. B.; Liu, Q. Q.; Zhao, J. G.; Yang, L. X.; Yu, Y.; Yu, R. C.; Katsura, T.; Shatskiy, A.; Ito, E. *Proc. Natl. Acad. Sci. U.S.A.* **2008**, *105*, 7115.
(30) Cheng, J. G.; Alonso, J. A.; Suard, E.; Zhou, J. S.; Goodenough, J. B. *J. Am. Chem. Soc.* **2009**, *131*, 7461.
(31) Find-It: Inorganic Crystal Structure Database (ICSD); Fachinformationszentrum (FIZ), Karlsruhe, Germany, 2010.
(32) Aguadero, A.; de la Calle, C.; Alonso, J. A.; Escudero, M. J.; Fernández-Díaz, M. T.; Daza, L. *Chem. Mater.* **2007**, *19*, 6437.
(33) Minh, N. V.; Yang, I. S. *Vib. Spectrosc.* **2006**, *42*, 353.
(34) Martín-Carrón, L.; de Andrés, A.; Martínez-Lope, M. J.; Casais, M. T.; Alonso, J. A. *J. Alloys Compd.* **2001**, *323*—*324*, 494.
(35) Nemudry, A.; Weiss, M.; Gainutdinov, I.; Boldyrev, V.; Schöllhorn, R. *Chem. Mater.* **1998**, *10*, 2403.